ADVANCES IN ATMOSPHERIC SCIENCES, VOL. 36, AUGUST 2019, 811–822

• **Original Paper** •

Simulated Influence of the Atlantic Multidecadal Oscillation on Summer Eurasian Nonuniform Warming since the Mid-1990s

Xueqian SUN[1,4], Shuanglin LI[*1,2,4], Xiaowei HONG[1], and Riyu LU[3,4]

[1]*Climate Change Research Center, Institute of Atmospheric Physics, Chinese Academy of Sciences, Beijing* 100029*, China*

[2]*Department of Atmospheric Science, China University of Geosciences, Wuhan* 430074*, China*

[3]*State Key Laboratory of Numerical Modeling for Atmospheric Sciences and Geophysical Fluid Dynamics, Institute of Atmospheric Physics, Chinese Academy of Sciences, Beijing* 100029*, China*

[4]*College of Earth and Planetary Sciences, University of Chinese Academy of Sciences, Beijing* 100049*, China*

(Received 18 December 2018; revised 18 March 2019; accepted 19 April 2019)

ABSTRACT

Based on ensemble experiments with three atmospheric general circulation models (AGCMs), this study investigates the role of the Atlantic Multidecadal Oscillation (AMO) in shaping the summer nonuniform warming over the Eurasian continent since the mid-1990s. The results validate that the positive-phase AMO can indeed cause nonuniform warming, with predominant amplified warming over Europe–West Asia and Northeast Asia, but with much weaker warming over Central Asia. The underlying mechanism is then diagnosed from the perspective that the boundary forcing modulates the intrinsic atmospheric variability. The results highlight the role of the Silk Road Pattern (SRP), an intrinsic teleconnection pattern across the subtropical Eurasian continent propagating along the Asian jet. The SRP can not only be identified from the AGCM control experiments with the climatological sea surface temperature (SST), but can also be simulated by the AMO-related SST anomaly (SSTA) forcing. Furthermore, diagnostic linear baroclinic model experiments are conducted, and the results suggest that the SRP can be triggered by the AMO-related tropical diabatic heating. The AMO-triggered SRP-like responses feature anticyclonic circulations over Europe–West Asia and Northeast Asia, but cyclonic circulation over Central Asia. These responses cause increased warm advection towards Europe–West Asia and Northeast Asia, reduced precipitation and cloud cover, and then increased downward shortwave radiation. This increased warm advection and increased downward shortwave radiation together cause amplified warming in Europe–West Asia and Northeast Asia. The situation is opposite for Central Asia.

Key words: Atlantic Multidecadal Oscillation, nonuniform warming, Silk Road Pattern

Citation: Sun, X. Q., S. L. Li, X. W. Hong, and R. Y. Lu, 2019: Simulated influence of the Atlantic Multidecadal Oscillation on summer Eurasian nonuniform warming since the mid-1990s. *Adv. Atmos. Sci.*, **36**(8), 811–822, https://doi.org/10.1007/s00376-019-8169-z.

Article Highlights:

- This study validates the role of the Atlantic Multidecadal Oscillation (AMO) in shaping the summer nonuniform warming over Eurasia.
- The possible mechanism for the AMO influence on the Eurasian nonuniform warming was proposed in terms of the SRP.
- The AMO-triggered SRP-like responses feature opposite circulations over Europe–West Asia, Northeast Asia, and Central Asia, leading to opposite changes in temperature advection, precipitation and cloud cover. Then nonuniform warming happened.

1. Introduction

After the mid-1990s, Eurasian surface air temperature (SAT) in summer shows a nonuniform warming pattern (Hong et al., 2017; also Fig. 1 here). The warming amplitude, expressed as the difference in regional-averaged SAT in 1997–2015 minus that in 1979–96 is 1.02°C, 1.08°C and 0.58°C over Europe–West Asia, Northeast Asia and Central Asia, respectively. There is a remarkable amplified warming over Europe–West Asia and Northeast Asia, but much weaker warming over Central Asia. Furthermore, the warming is not only confined to the surface but also extends to the middle-lower troposphere (Fig. 1b). Due to the enormous economic

* Corresponding author: Shuanglin LI
Email: shuanglin.li@mail.iap.ac.cn

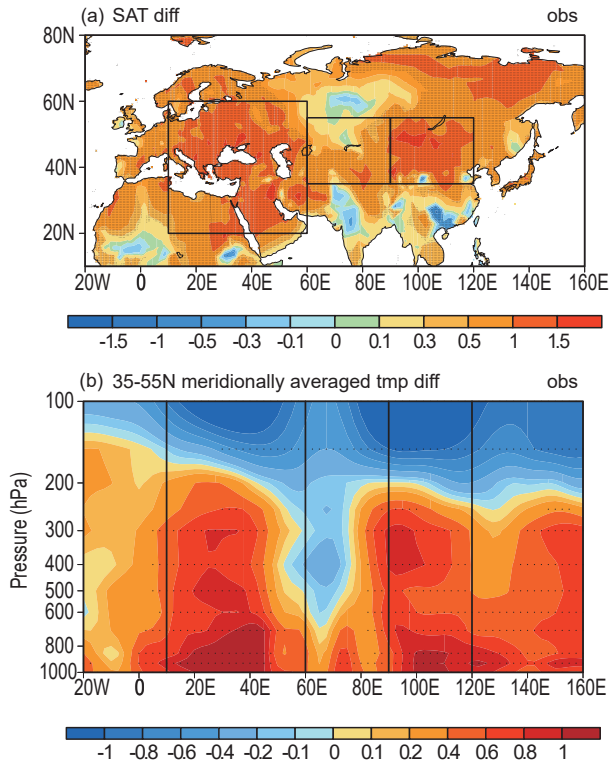

Fig. 1. (a) The JJA-mean SAT differences (1997–2015 minus 1979–96) (shading; units: °C). The three boxes represent Europe–West Asia (20°–60°N, 10°–60°E), Central Asia (35°–55°N, 60°–90°E) and Northeast Asia (35°–55°N, 90°–120°E), respectively. The trend of the SAT during 1901–2015 is removed before calculating the difference. (b) As in (a) but for pressure–longitude cross sections of meridionally averaged (35°–55°N) air temperature difference (shading; units: °C). Dotted areas indicate statistical significant at the 95% confidence level. The black lines correspond to the longitude of the three boxes in (a).

value and large population, the predominant warming over Europe–West Asia and Northeast Asia has caused wide public attention.

What caused this nonuniform warming is intriguing but unclear. Previous studies suggest that the Atlantic Multidecadal Oscillation (AMO) may be one candidate, since the variations in Eurasian SAT are closely related with it. For instance, Li and Bates (2007) and Wang et al. (2009) suggested the positive phase of the AMO can give rise to increased air temperatures over East Asia in both observations and models. Ionita et al. (2012, 2013) illustrated the warmer summer temperatures over Europe are related to the long-term changes in the AMO. Beyond these, Hao et al. (2016) revealed not only the effect of the AMO on the Eurasian continent, but also an obvious asymmetry in the winter SAT over the Central Eurasia region (30°–50°N, 30°–70°E) with respect to the AMO phase. Thus, the role of the AMO cannot be excluded.

Based on observational analysis, Hong et al. (2017) proposed that the nonuniform warming is related to the phase shift of the AMO. In detail, the AMO modulates the activity of the summer quasi-zonally propagating teleconnection wave train, the Silk Road Pattern (SRP), which is guided by the summer Asian jet and exhibits a wave-train-like structure along the ancient silk trade road across the Mediterranean, West Asia, Central Asia and East Asia (Lu et al., 2002; Enomoto et al., 2003; Kosaka et al., 2012; Hong and Lu, 2016). There is a substantial correspondence of the two predominant warming regions in Europe–West Asia and Northeast Asia to the two anticyclonic circulation anomalies constituting the SRP. Due to the turn of the AMO phase from negative to positive in the mid-1990s, the associated SRP shifted and caused positive geopotential heights over Europe–West Asia and Northeast Asia, but negative geopotential height anomalies over Central Asia. The effect of the SRP phase shift overlapped global warming and caused nonuniform warming.

However, Hong et al. (2017)'s observational analysis was based on limited instrumental records that covered just one and a half phase periods of the AMO. Moreover, in addition to the AMO, other factors (e.g., greenhouse gases, Pacific Decadal Oscillation) can also affect the changes in SAT. So, it is necessary to isolate the AMO's effect alone by model experiments. Thus, the present study aims to verify the AMO's role in shaping the Eurasian nonuniform warming by taking advantage of three AGCM experiments forced by the AMO-related sea surface temperature anomaly (SSTA). Further, the underlying mechanism of the AMO affecting the nonuniform warming is investigated.

The remaining part of this paper is organized as follows: Section 2 introduces the data, methods and models used in this study. The modeled SAT response to the AMO is displayed in section 3. Section 4 discusses the mechanism by which the SRP influences the SAT. Section 5 describes the relationship between the AMO and SRP. Finally, a summary and discussion are presented in section 6.

2. Data and methods

2.1. *Data*

The observed SAT data used are the monthly land air temperature dataset (version 3.24) developed by the Climate Research Unit (CRU), University of East Anglia, UK (Harris et al., 2014), with a resolution of $0.5° \times 0.5°$ from 1901 to 2015. Reanalysis of multiple-level monthly mean wind and air temperature with a $2.5° \times 2.5°$ horizontal resolution from the National Centers for Environmental Prediction–National Center for Atmospheric Research (NCEP/NCAR) (Kalnay et al., 1996) through 1981 to 2010 are used to derive the observational basic flow for the diagnostic linear baroclinic model (LBM) experiments. The observational monthly precipitation data are from the program named Visualize Precipitation Reconstruction (PREC) (Chen et al., 2004), which has a resolution of $2.5° \times 2.5°$ and spans the period 1948–2017. The SSTA data are from the Kaplan Extended SST spanning 1856–2016 (Kaplan et al., 1998). The Atlantic Multidecadal Oscillation Index (AMOI) is defined as the annual averaged

SSTA in the North Atlantic basin (0°–60°N, 75°–7.5°W) (Enfield et al., 2001; Wang et al., 2009). The linear trend of SST is removed and a nine-point running-mean is used to obtain the decadal components when calculating the AMO index.

In addition to these observational data, the model experimental data gathered previously by Wang et al. (2009) from three AGCMs are used to obtain the atmospheric responses to the AMO. The three AGCMs are the Atmospheric Model (AM2) of the GFDL (Geophysical Fluid Dynamics Laboratory), the Global Forecasting System (GFS) of the NCEP, and the Community Climate Model, version3.0 (CCM3), of NCAR. Two sets of ensembles—the control ensemble, whose runs are forced by the climatological SST seasonal cycle, and the SSTA ensemble with an AMO SSTA described as the SST difference in warm-phase AMO (1935–55) and cold-phase AMO (1970–90) added on to the climatological seasonally evolving SST—are performed in each model. The SSTA pattern used in the AGCM experiments is shown in Fig. 2. For AM2, each ensemble has four members with an integration of 25 years. To allow for model spin-up, the first model year in the integration is abandoned, resulting in a total of 96 model years available in each ensemble. For CCM3, two ensembles with 40 members each are performed. For GFS, the control ensemble is formed from 40 runs and the SSTA ensemble is formed from 60 runs. The runs in CCM3 and GFS all start from different initial fields and are integrated for 13 months from September to the following September. Thus, a total of 40 model years are available in each ensemble for CCM3, and a total of 40 or 60 model years are available in the control or SSTA ensemble for GFS, respectively. The further details about the experiments, readers are referred to Li and Bates (2007) and Wang et al. (2009). The experimental variables used in this study include SAT, air temperature, precipitation, meridional and zonal wind components (v and u), and geopotential height. As before, the atmospheric response to the AMO is quantified by the difference of the variables in the AMO-SSTA forced sensitive ensembles minus those in the control ensembles. The significance is determined by the Student's t-test.

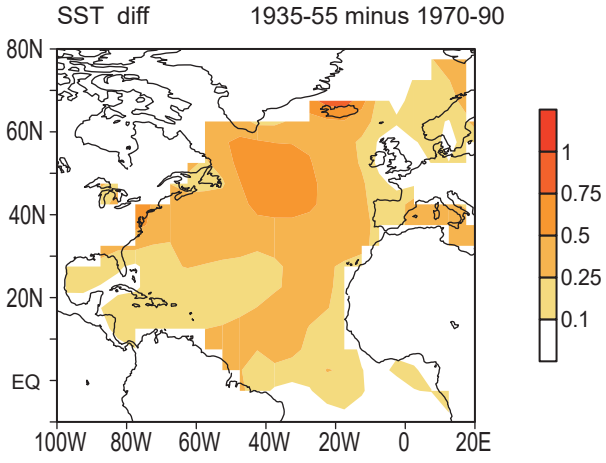

Fig. 2. The annual mean SSTA difference between the warm AMO (1935–55) and the cold AMO (1970–90). Units: °C. The monthly SSTA is detrended and a 10-year running-mean filter is adopted to calculate the difference.

2.2. *Methods*

The main statistical tools used are composite, EOF and linear regression analyses. Composite analysis is used to derive the SAT anomalies linked to the AMO. EOF analysis is utilized to obtain the SRP-like wave train. Regression analysis is used to obtain the linear component related to the SRP.

One diagnosis with the thermodynamic budget equation is conducted to understand the formation of anomalous SAT. The thermodynamic energy equation in the P-coordinate is written as

$$\frac{\partial T}{\partial t} = -\left(u\frac{\partial T}{\partial x} + v\frac{\partial T}{\partial y}\right) + (\Gamma_\mathrm{d} - \Gamma)\omega + \frac{1}{c_p}\dot{Q}\,, \tag{1}$$

where T is the air temperature; u, v and ω are the zonal, meridional and vertical velocity, respectively; Γ_d is the dry adiabatic lapse rate; Γ is the temperature lapse rate; c_p is the specific heat of air and $\dot{Q}$ is the diabatic heating rate. The three terms on the right-hand side represent horizontal temperature advection, vertical temperature advection, and diabatic heating, respectively. The Γ_d and Γ are calculated separately as

$$\Gamma_\mathrm{d} = \frac{\gamma_\mathrm{d}}{\rho g} = \frac{R\gamma_\mathrm{d}}{g}\frac{T}{P} = 0.293\frac{T}{P}\,, \tag{2}$$

and

$$\Gamma = \frac{\partial T}{\partial P} = \frac{T(z-1) - T(z+1)}{P(z-1) - P(z+1)}\,, \tag{3}$$

where the atmospheric density (ρ) is equivalent to $P/(RT)$, the gravitational acceleration (g) is 9.8 kg m^{-2}, the gas constant (R) of the dry air is 2.87×10^2 m^2 s^{-1} K^{-1}, and the dry adiabatic lapse rate in the Z-coordinate (γ_d) is 0.01 K m^{-1}. P is atmospheric pressure. Variable z refers to the vertical level number of the atmosphere.

In order to isolate the direct effect of AMO-related diabatic heating, diagnostic experiments with an LBM are carried out. The LBM can be referred to in Li (2004) and Shao et al. (2018). In the LBM, diabatic heating and transient momentum flux convergence are treated as forcing, and atmospheric direct responses to these forcings are obtained by forward-integrating the LBM to approximate a steady solution under a background basic flow and appropriate dispersion and diffusion. For the observational diagnostics, the background basic state is calculated as the summer (June–July–August, JJA) mean climatology during 1981–2000 based on the NCEP–NCAR reanalysis. For the diagnostics of AM2's atmosphere, the background basic state is derived from the model's control ensemble with the climatological monthly SST forcing. In order to obtain a stable response, Rayleigh friction and Newtonian damping as well as biharmonic diffusion and thermal diffusion coefficients are set the same as in Li (2004), except for the Rayleigh friction and Newtonian damping at the lowest level for AM2, which has a different value (7 days) $^{-1}$. It takes about 35 days for the LBM response to reach a steady state under these damping

terms, and we choose the last five days of a 40-day integration to represent the atmospheric linear responses to forcing.

3. Modeled SAT response

The modeled SAT responses to the AMO SST anomaly in the three AGCMs are analyzed first. Because of a qualitative similarity among the three AGCMs, only the results from AM2 are presented in detail, and we give a more general description for the other two models. From Fig. 3, visually, there is a nonuniform warming in the midlatitudinal Eurasian continent, with amplified warming in Europe–West Asia (from the Mediterranean, Black Sea, to the Caspian Sea) and East Asia, and with weaker warming in Central Asia. There are, however, some differences from the observational composite (compare Fig. 3a and Fig. 1a)—for instance, stronger enhanced warming over northwestern Russia and southeastern China—but the modeled responses bear a qualitative resemblance to the observation. The mid–lower tropospheric warming over Europe–West Asia and East Asia also resembles the observation (Fig. 3b).

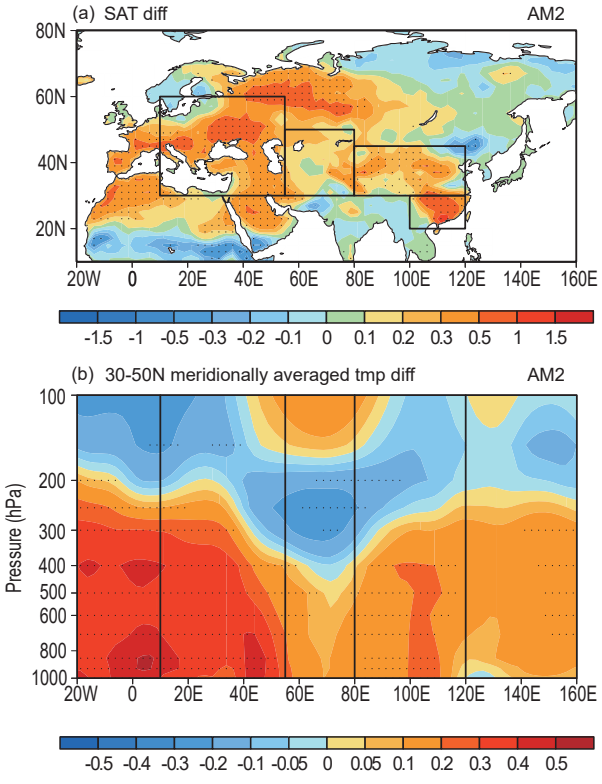

Fig. 3. (a) Modeled summer (JJA) SAT response to the AMO SSTA for AM2. The four boxes represent Europe–West Asia (30°–60°N, 10°–55°E), Central Asia (30°–50°N, 55°–80°E), East Asia (30°–45°N, 80°–120°E) and Southeast China (20°–30°N, 100°–120°E), respectively. (b) As in (a) but for the 30°–50°N meridionally averaged air temperature response. The black lines correspond to the longitude of the three boxes representing Europe–West Asia, Central Asia and East Asia in (a). Dotted areas represent statistical significant at the 90% confidence level. Units: °C.

Figure 4 displays the SAT responses in CCM3 and GFS. The responses in these two models are qualitatively similar to those in the observation or AM2, although the intensity and position of the predominant warming areas are slightly altered. In CCM3, the warming in western Europe is less significant, with a decreased amplitude (compare Fig. 1a and Fig. 4a). In GFS, the warming observed in Northeast Asia moves westwards by about 10° of longitude and has a weakened amplitude (compare Fig. 1a and Fig. 4b). Nevertheless, the SAT responses in both models show a nonuniform warming pattern.

From the above results, it is evident that the AMO has exerted substantial effects on the Eurasian nonuniform warming since the mid-1990s. When the AMO is in positive phase, there is significantly amplified warming in Europe–West Asia and East Asia, while relatively weaker warming in Central Asia.

It is known that model deficiencies may distort the modeled atmospheric response. The simulated response to forcing in AGCMs strongly relies on and projects upon the internal variability modes of the model's atmosphere, rather than bears a new mode of variability (e.g., Ting and Peng, 1995; Peng and Whitaker, 1999). So, the reliability of the modeled responses depends on whether the model reproduces intrinsic variability in the same way as in the observed atmosphere (Li, 2004). Hong et al. (2017) revealed that the observed

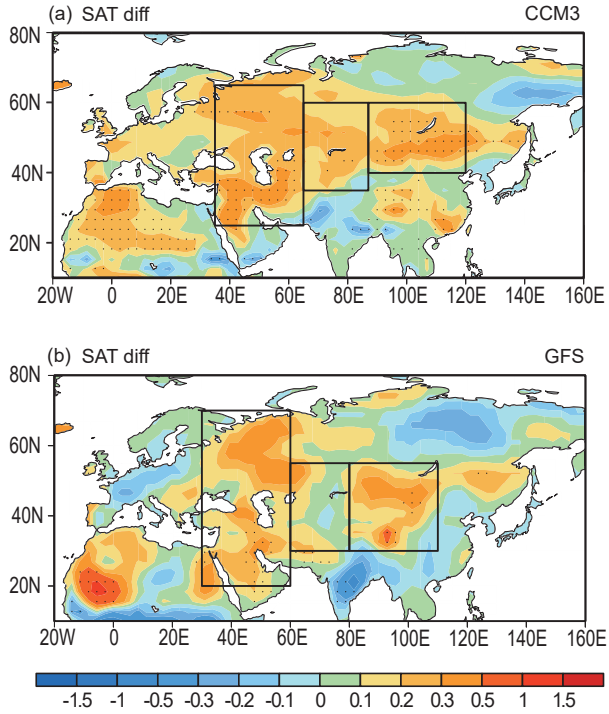

Fig. 4. As in Fig. 3a but for (a) CCM3 and (b) GFS. The three boxes represent Europe–West Asia [(25°–65°N, 35°–65°E) in (a), (20°–70°N, 30°–60°E) in (b)], Central Asia [(35°–60°N, 65°–87°E) in (a), (30°–55°N, 60°–80°E) in (b)] and Northeast Asia [(40°–60°N, 87°–120°E) in (a), (30°–55°N, 80°–110°E) in (b)), respectively. Dotted areas represent statistical significant at the 90% confidence level.

nonuniform warming in the Eurasian continent is closely related with the SRP. So, in the next section, we focus on whether the three AGCMs can reproduce the observed SRP teleconnection reasonably over the Eurasian continent, and investigate the possible mechanism for the AMO influence on the Eurasian nonuniform warming in terms of the SRP.

4. Mechanisms

4.1. *SRP*

Based on observational analysis, Hong et al. (2017) suggested that the SRP may have played an important role in the Eurasian summer nonuniform warming. To obtain the SRP, an EOF analysis is applied to the NCEP–NCAR reanalysis 200-hPa meridional wind anomalies for 37 summers (1979–2015) within the domain (20°–60°N, 0°–150°E). The leading EOF mode explains 25.8% of the total variance and features a quasi-zonal wave train extending from western Europe across the entire Eurasian continent via the Mediterranean, West Asia, Central Asia and East Asia with alternating positive and negative centers (Fig. 5a). When the EOF analysis is performed over a larger domain (5°–75°N, 30°W–180°E), a highly similar leading EOF pattern is obtained (not shown). Such a result suggests that the SRP is not sensitive to the region used. Thus, the corresponding principle component of the leading EOF is defined as the SRP Index (SRPI). The SRP-related SAT anomalies show opposite changes in temperature over Europe–West Asia and Northeast Asia to those over Central Asia (Fig. 5b). The regions with positive SAT anomalies correspond well to the regions with amplified warming, implying that the SRP plays an important role in shaping the Eurasian nonuniform warming (compare Fig. 1a and Fig. 5b).

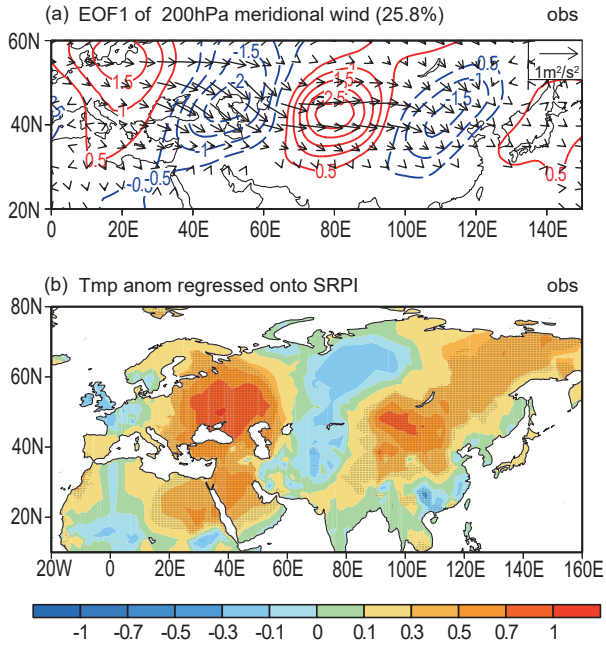

Fig. 5. (a) The first EOF mode for NCEP–NCAR reanalysis 200-hPa seasonal (JJA) meridional wind anomalies (contours; units: m s^{-1}), and the Plumb wave activity flux (vectors; units: m^2 s^{-2}) regressed onto the first principal component of the EOF. Contour intervals are 0.5 m s^{-1}. (b) The surface land temperature anomaly regressed onto the SRPI. Dotted areas indicate statistical significant at the 95% confidence level.

In order to examine whether the AGCMs' atmospheres reproduce the SRP-like intrinsic variability, the simulations from their control experiments with only climatological monthly SST forcing are utilized to perform EOF analysis. The domain for the EOF and the definition for the SRPI are identical to the observational one. Again, when a larger domain (5°–75°N, 30°W–180°E) is used to conduct the EOF analysis, the resultant leading pattern does not alter evidently. For the three AGCMs, their respective leading EOF modes (not shown) bear a resemblance to the observed SRP, with an overall zonally oriented positive–negative–positive–negative structure, although the detailed positions of the lobes constituting the SRP exhibit certain differences in comparison to the observed (compare Fig. 5a and Figs. 6a, c and e). Besides, the SRP-related SAT anomalies in these AGCMs are characterized by nonuniform warming or cooling in Eurasia, with a zonally warm–cold–warm structure, qualitatively similar to the observed (compare Figs. 6b, d and f with Fig. 5b). For AM2, the wave-train lobes' positions are similar to the observation, although their intensity is weaker (compare Fig. 6a and Fig. 5a). The SAT anomalies regressed against the SRPI also bear a resemblance to the observation (compare Fig. 6b and Fig. 5b). The stronger warming in Europe and the moderate warming from the Tibetan Plateau southeastwards to Southeast China correspond to the two positive temperature anomalies in the regression, while the negative anomalies over Central Asia correspond to the weakened warming (compare Fig. 6b and Fig. 3a).

For CCM3, the intensity and the location of the wave-train centers and the anomalies related with the SRP in Europe–West Asia, Central Asia and Northeast Asia are nearly the same as in the observation (compare Fig. 6c and Fig. 5a, Fig. 6d and Fig. 5b). The regressed positive SAT anomalies over northern Europe and East Asia are consistent with the amplified warming. The negative temperature anomaly in Central Asia corresponds to weak warming (compare Fig. 6d and Fig. 4a).

For GFS, the SRP wave train is still clear, albeit shifted to the east and north somewhat and with a swift decay of the intensity of the centers in East Asia compared with the observation (compare Fig. 6e and Fig. 5a). Corresponding to the shift, the maximum of the temperature anomalies over Europe in the regressions shifts to the Ural Mountains, and the cooling in Central Asia shifts eastwards, with the minimum between Lake Balkhash and Lake Baikal, and the warming over East Asia in the observational regression becomes less evident (Fig. 6f).

To check whether the AMO SST anomaly acting as a forcing can excite the SRP-like wave train, the meridional wind responses in the three AGCMs are displayed in Fig. 7. The responses in each AGCM feature a zonally elon-

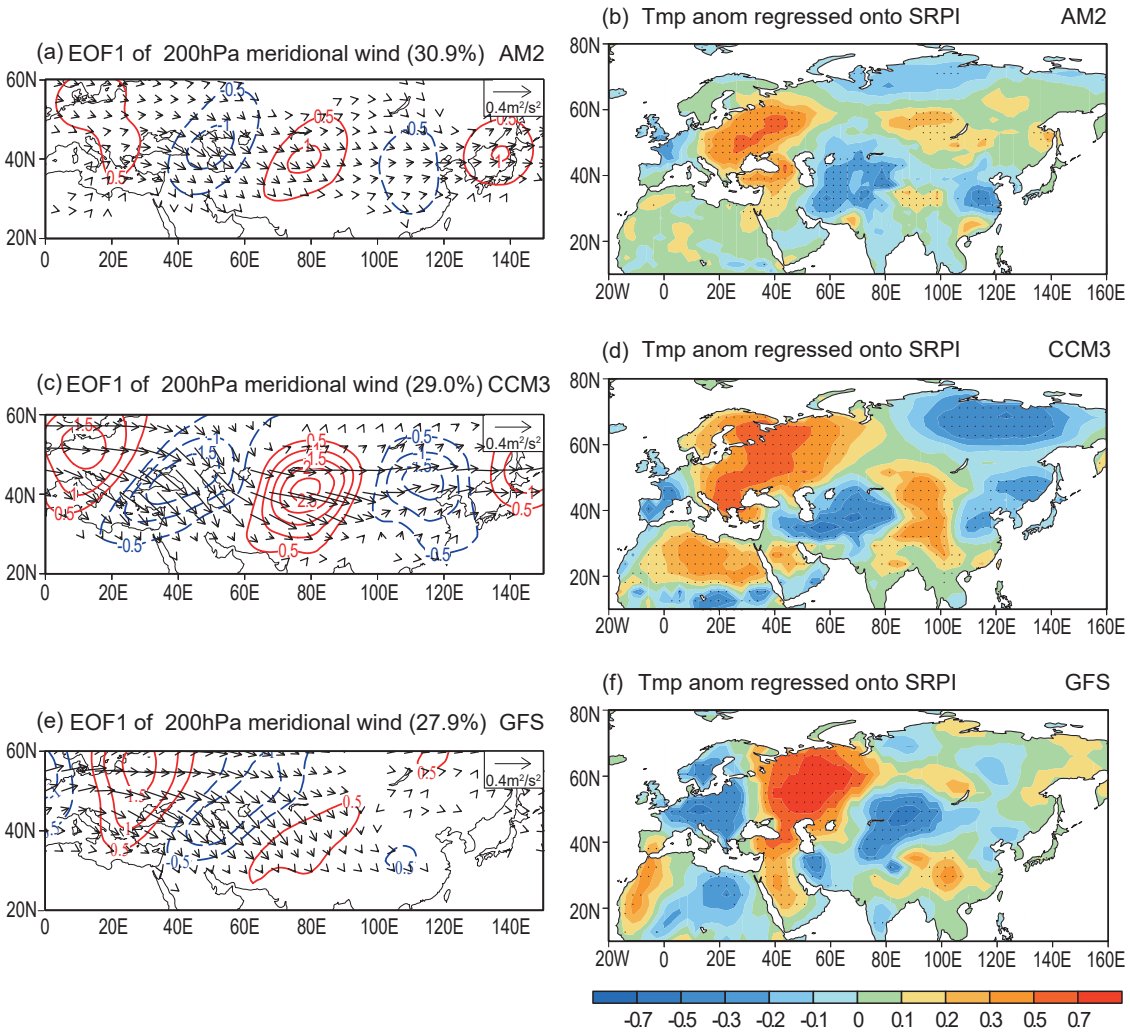

Fig. 6. As in Fig. 5 but for (a, b) AM2's, (c, d) CCM3's, and (e, f) GFS's control runs. The variance contribution rates of the first mode in the three AGCMs are 30.9%, 29.0% and 27.9%, respectively. Dotted areas indicate statistical significant at the 90% confidence level.

gated wave train propagating downstream along the subtropical Eurasian continent. It indicates that the SRP can be excited by the AMO-related SST anomaly.

In summary, the observed SRP variability is reproduced in the three AGCMs well, and the SRP features a zonally oriented structure with alternative positive and negative centers in mid-latitudinal Eurasia for both the observation and AGCMs experiments. Furthermore, the SRP-like wave train can be triggered by the AMO SST anomaly. The SAT anomalies associated with the wave train pattern exhibit an overall zonally oriented warm–cold–warm variation, indicating that the SRP is of great importance for the nonuniform changes in temperature over the Eurasian continent.

4.2. *Related atmospheric circulation*

Before the detailed mechanism for the SRP inducing nonuniform SAT variation is explored, the SRP-related atmospheric circulation is analyzed. The results from AM2 are focused upon in view of their resemblance to those from the two other models. Figure 8a displays the regressions of 850-hPa air temperature, geopotential height and horizontal wind onto the SRPI derived from AM2's control runs. The SRP-related air temperature overall resembles the SRP-related SAT anomalies, with positive anomalies in Europe–West Asia and Northeast Asia but negative anomalies in Central Asia (compare Fig. 8a and Fig. 6b). This substantial consistency of the 850-hPa air temperature anomalies and SAT anomalies corresponds to the vertically consistent warming through the lower–middle troposphere (Fig. 3b). The 200-hPa geopotential height anomalies associated with the SRP (Fig. 8b) are positive over Europe and Northeast Asia, which are consistent with those at 850 hPa and implies an equivalent-barotropic structure. However, Central Asia is different, with negative anomalies at 200 hPa and weak positive anomalies at 850 hPa, indicating a baroclinic structure. A similar correspondence also exists in observations (Hong et al., 2017). The difference in vertical structure over Central Asia from those over the other regions may suggest a different origination of their anomalous air temperature, since the positive geopotential height anomalies through the whole troposphere may be

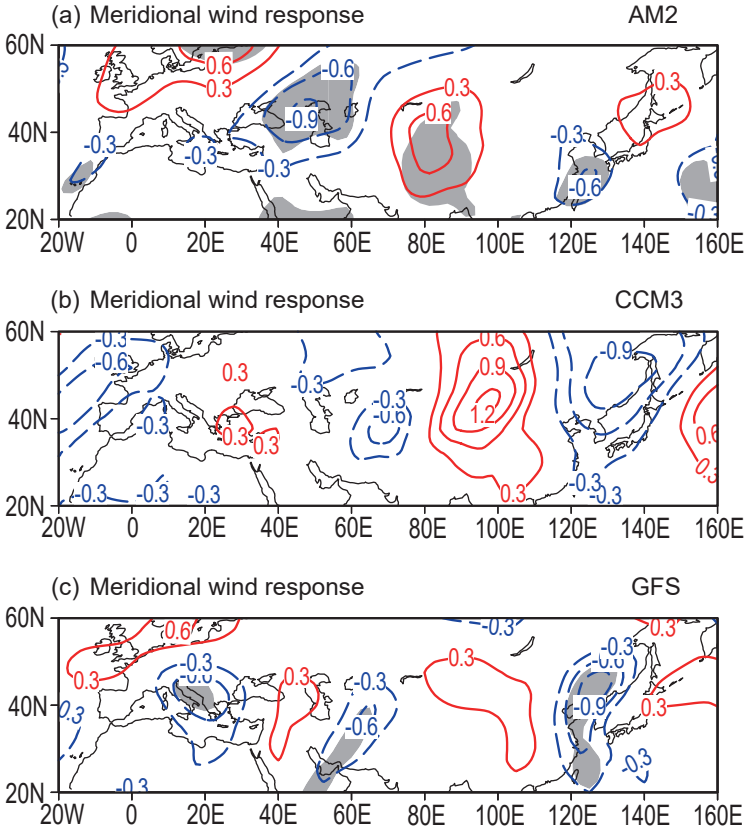

Fig. 7. Modeled summer (JJA) meridional wind response to the AMO SSTA for (a) AM2, (b) CCM3 and (c) GFS. Units: m s^{-1}. Shaded areas indicate statistical significant at the 90% confidence level.

conducive to maintaining clear weather and allowing more solar radiation to reach the surface.

Generally, the equivalent-barotropic structure over the mid–high latitudes is maintained by dynamical factors like the synoptic transient vorticity forcing, while a baroclinic structure is usually maintained by thermodynamic factors like diabatic heating. Since latent heating release is the dominant component of diabatic heating, the SRP-related rainfall anomalies are displayed (Fig. 8c). The rainfall anomalies bear a correspondence to the SAT anomalies, with less and more precipitation versus positive and negative SAT, respectively (compare Fig. 8c and Fig. 6b). This indicates that the warming in Europe and Northeast Asia originates more from the interaction of dynamical and thermal forcing, while the warming in Central Asia is mainly from diabatic heating. Precipitation may influence SAT through cloud-radiation effects. Decreased precipitation corresponds to decreased coverage of cloud, permits more shortwave radiation to reach the surface, and favors regional warming.

4.3. *Thermal advection*

Temperature advection is usually an important factor affecting the changes in temperature (e.g., Sun et al., 2008). Thus, the SRP-related horizontal temperature advection at 1000–700 hPa and vertical advection throughout the whole troposphere are calculated to understand the formation of anomalous SAT in Fig. 6b. Figure 9a shows the distribution of vertical mean horizontal temperature advection associated with the SRP. It can be seen that Europe, Central Asia and Northeast Asia feature warm, cold and warm advection, respectively, corresponding to the warm, cold and warm SAT anomalies derived from the SRPI regression (compare Fig. 6b and Fig. 9a). The predominant warm advection from the Caspian Sea to the northwest and from North China to Lake Baikal contributes to the warm anomalies in western Europe and Northeast Asia, respectively. Simultaneously, the cold advection from northern Europe southeastwards to eastern Central Asia leads to the cold SAT anomalies there. However, the SRP also causes warm advection in western and central parts of Central Asia and cold advection in southeastern China. Therefore, both the cold SAT anomalies in western and central parts of Central Asia and the warm anomalies in southeastern China cannot be fully explained in terms of horizontal advection.

The distribution of vertically averaged vertical advection shows that the SRP produces warm advection in northern Europe, Northeast Asia and southeastern China, which may be related to enhanced adiabatic descent (Figs. 9b and c). The regions with warm advection are in general consistent with the regions with warm SAT anomalies. The cold advection in western and central parts of Central Asia can account for the cold SAT anomalies there.

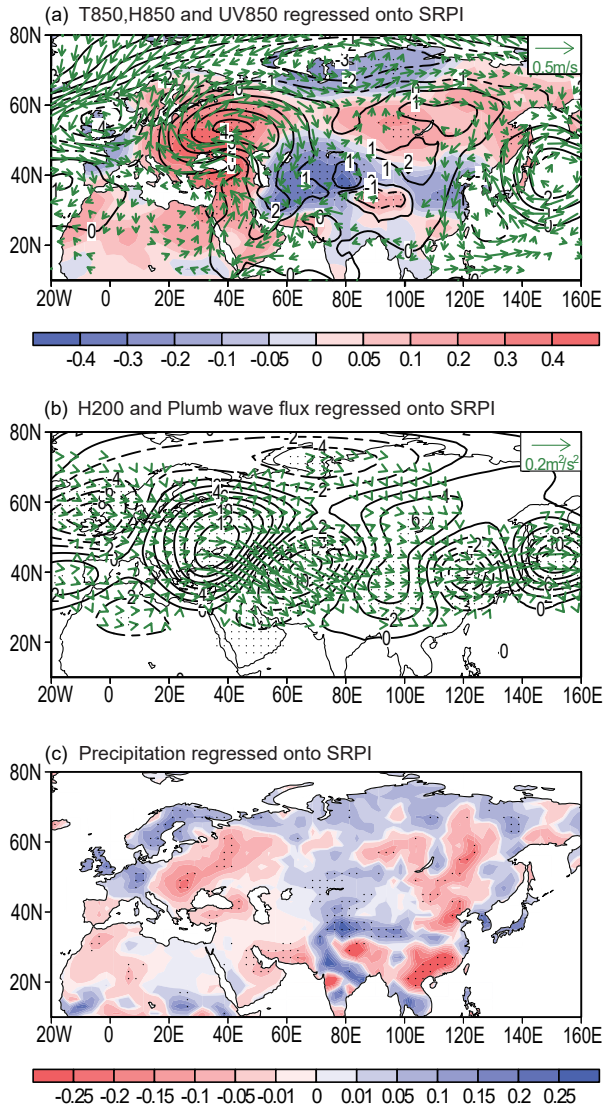

Fig. 8. (a) The seasonal (JJA) 850-hPa air temperature (T850) anomalies (shading; units: °C), geopotential height (H850) anomalies (contours; units: gpm), and horizontal wind (vectors; m s^{-1}) regressed against the SRPI in AM2's control runs. (b) As (a) but for the 200-hPa geopotential height (H200) anomalies (shading; units: gpm) and Plumb wave activity flux anomalies (vectors; units: m^2 s^{-2}). (c) As in (a) but for the precipitation anomaly (units: mm d^{-1}). Dotted areas represent statistical significant at the 90% confidence level.

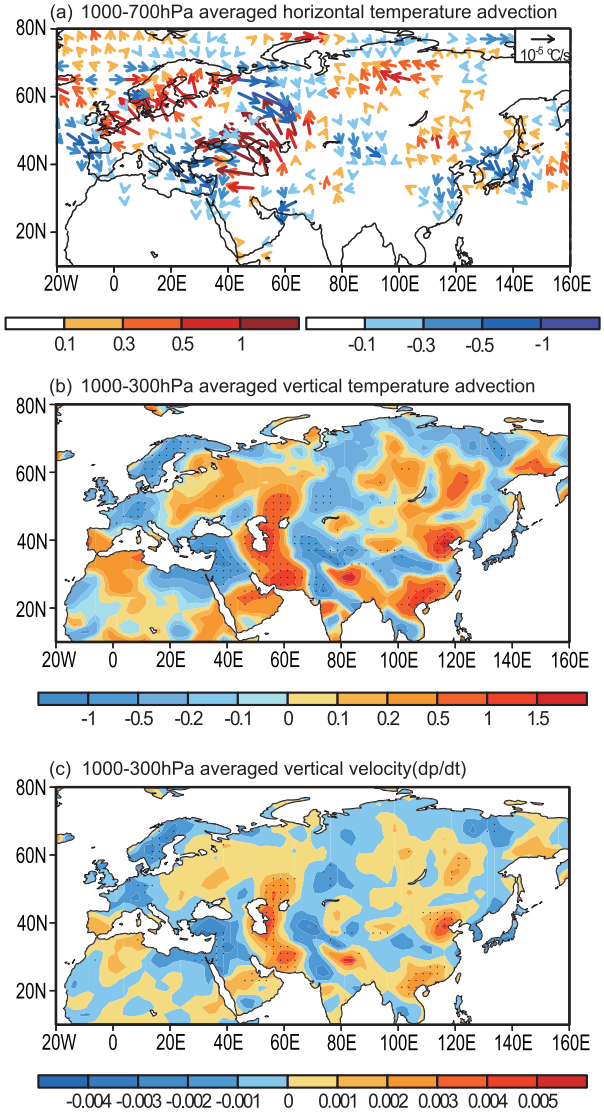

Fig. 9. The (a) 1000–700-hPa vertical mean horizontal temperature advection [units: 10^{-7} °C s^{-1}; red (blue) vectors represent warm (cold) advection], (b) 1000–300-hPa vertical mean vertical temperature advection (units: 10^{-5} °C s^{-1}) and (c) vertical velocity (units: Pa s^{-1}) in AM2's control runs regressed against the SRPI during June–August. Dotted areas represent statistical significant at the 90% confidence level.

5. Origination of the SRP

In order to verify the AMO's role in shaping the Eurasian nonuniform warming through modulating SRP activity, we carry out LBM experiments to obtain the direct atmospheric response to the diabatic heating related to the AMO. It is well known that the release of latent heat is dominant in the total diabatic heating, and rainfall anomalies can represent the column vertically integrated latent heating (e.g., Hagos et al., 2010). Therefore, we utilize the AMO-related rainfall in the tropical Atlantic to mimic the diabatic heating anomaly associated with the AMO. Figure 10a displays the spatial distribution of rainfall regression over the Atlantic against AMOI in the observation. The positive phase of the AMO brings increased rainfall over the Sahel, northern Brazil and Latin America, but decreased rainfall over tropical South America and Northeast Brazil. The simulated precipitation response in AM2 (Fig. 10b) closely resembles the observation in spite of weaker amplitudes in the Sahel and in Northeast Brazil. The rainfall pattern in both the observation and AM2 implies a northward shift of the summer Atlantic climatological ITCZ. The result is consistent with previous studies (Knight et al., 2006; Zhang and Delworth, 2006; Ting et al., 2009, 2011; Mohino et al., 2011; Han et al., 2016). The pre-

cipitation rate of 10 mm d^{-1} is approximately equal to the column-averaged latent heating rate of 2.5 K d^{-1} (e.g., Jin and Hoskins, 1995; Ting and Peng, 1995). The vertically averaged diabatic heating anomalies calculated by the precipitation anomalies are shown in Fig. 11. An idealized vertical heating profile is needed in the LBM and is based on Li et al. (2010). The maximum heating is at 400 hPa (Fig. 11c), which is consistent with the observed deep tropical convection (Yanai et al., 1973). The vertical heating profile in Fig. 11b has the same curve shape as Fig. 11a except for different values of the x-coordinates due to different amplitudes of the precipitation anomaly. So, just one profile is displayed.

Figure 12 shows the response of geopotential height and wind fields to the AMO-related tropical diabatic heating. For the observational basic state (Figs. 12a and b), there are positive geopotential height anomalies accompanied by anticyclonic circulation over Europe and Northeast Asia but negative geopotential height anomalies and cyclonic circulation

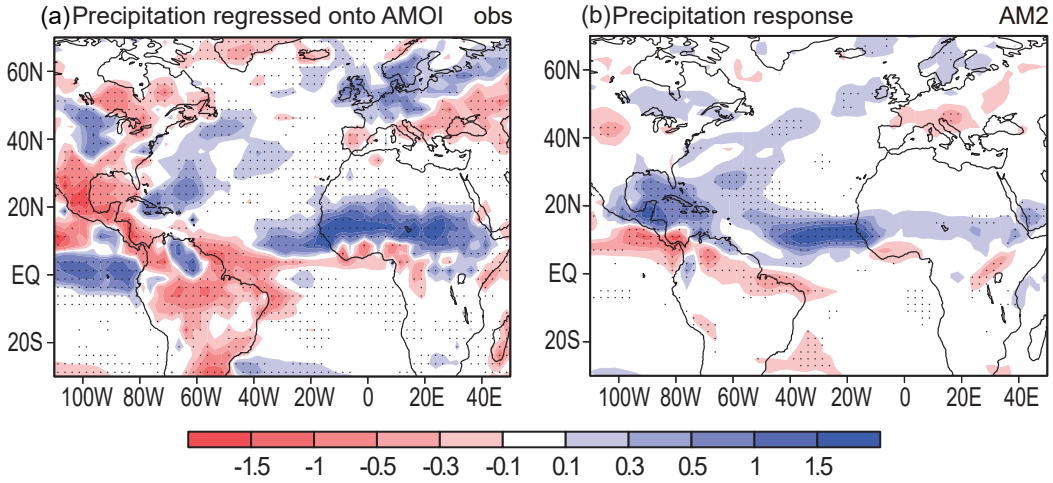

Fig. 10. The precipitation anomalies (units; mm d^{-1}) related to the AMO during summer (JJA) for (a) the observation and (b) AM2. For observation (a), the precipitation anomalies are regressed onto the AMO index during 1948–2017 based on the PREC dataset. For AM2 (b), the AMO-related anomalies are derived from the differences between the SSTA ensemble and control ensemble. Statistically significant anomalies at the 99% confidence level are dotted.

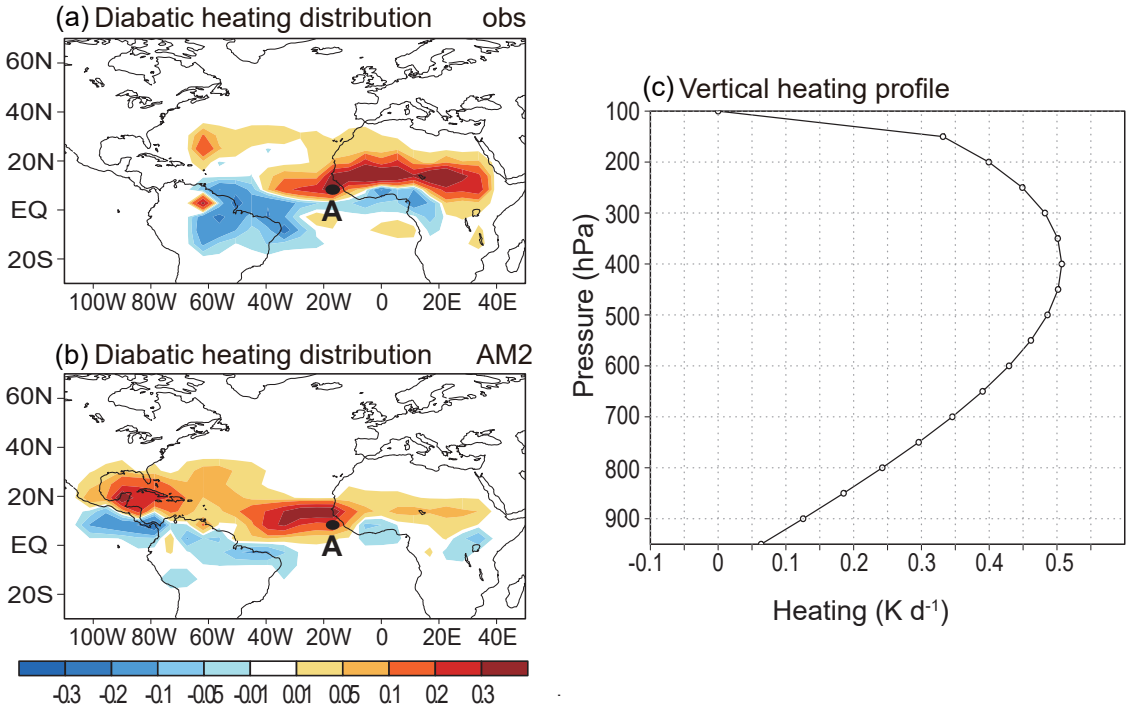

Fig. 11. Vertically averaged diabatic heating anomalies (units: K d^{-1}) for (a) the observation and (b) AM2 representing the SSTA-induced heating at the initial stage during the summer (JJA), the dot "A" represents a spot in the tropics and (c) the vertical heating profile for the dot "A" in (a).

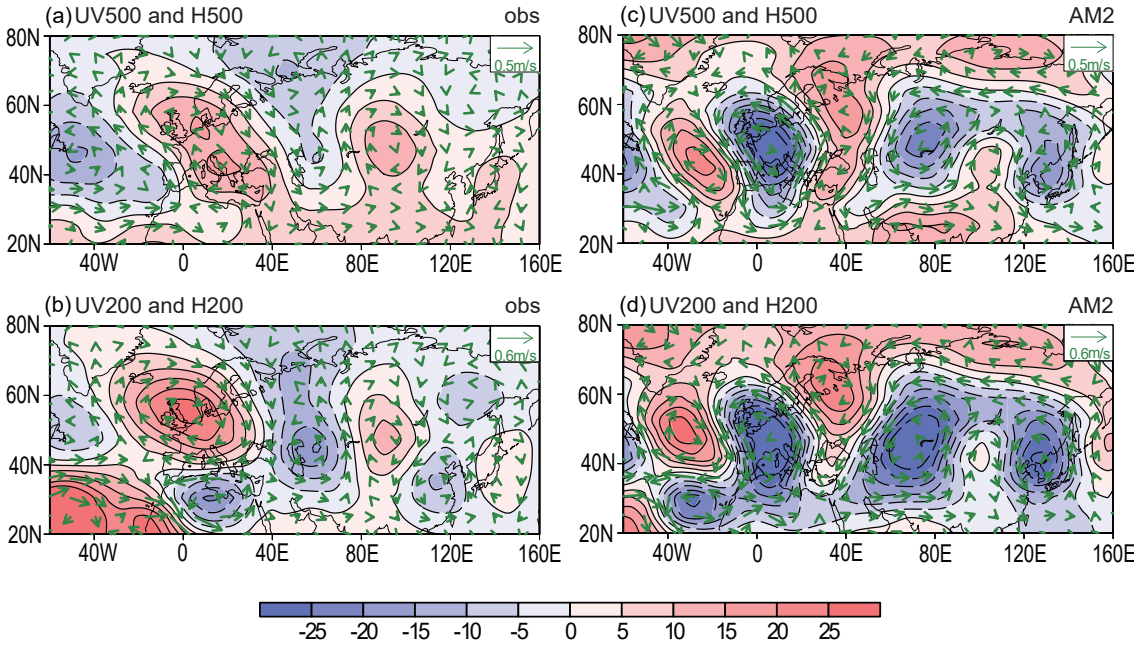

Fig. 12. LBM responses of wind (vectors; units: m s^{-1}) and geopotential height (shading and contours; units: gpm) at 500 hPa and 200 hPa for (a, b) the observation and (c, d) AM2.

over Central Asia at 500 hPa. Although the 200-hPa positive height anomalies over Europe shift west, the distribution of the circulation anomalies bears a resemblance to the observational composite in Hong et al. (2017). For the AM2 basic state (Figs. 12c and d), there are positive geopotential height anomalies and anticyclonic circulation over Europe and East Asia at both 500 hPa and 200 hPa (Figs. 12c and d). The LBM experiment results indicate that AMO-related abnormal heating in the tropical Atlantic may excite the formation of the Eurasian SRP.

6. Summary and discussion

This study has investigated the role of the AMO in shaping the Eurasian summer nonuniform warming since the mid-1990s through forcing-sensitive experiments in three AGCMs and diagnostic simulations in a linear baroclinic dry model. The results suggest that the phase shift of the AMO to positive since the mid-1990s can indeed cause SRP-like atmospheric anomalies, and result in Eurasian summer nonuniform warming. The overall consistency among the three AGCMs illustrates the robustness of the AMO's influence, although the models are not the most recent updated versions.

It is known that the reliability of the simulated response in AGCMs to external forcing strongly depends on the model's intrinsic variability. Whether the AGCMs used here reproduce the observed intrinsic variability was also analyzed. The results suggest that the SRPs in the models are qualitatively similar to the observed, indicating all three AGCMs reproduce the observed intrinsic variability well. This illustrates that the present results are physically reasonable.

Because the SRP can arise from internal climate variability or be triggered by the AMO, one may be concerned about the respective contributions of the intrinsic SRP-like variability and the SRP wave train triggered by the AMO SST anomaly to the observed nonuniform warming. In response to this concern, we conducted a supplementary analysis by using two longer series datasets—the 1901–2014 observational SAT and meridional wind component from CRU and the 20th Century Reanalysis (V2c), respectively. Such a longer series analysis provides the possibility to permit the signals triggered by various decadal external forcings to at least partly offset one another. The signal of global warming in the series can be removed by applying a detrending process. Thus, the atmospheric intrinsic SRP together with its individual contribution can be obtained by EOF and regression analyses of the longer series. From Fig. 13, the intrinsic SRP-like variability may have contributed 0.52°C over Europe–West Asia and 0.3°C in Northeast Asia. As such, the warmth over Europe–West Asia and Northeast Asia is remarkably reduced to 0.59°C and 0.76°C from 1.11°C and 1.06°C, respectively. In comparison, central Eurasia is less affected by intrinsic SRP-like variability. The contribution of the AMO is also calculated by regressions. The result indicates the SAT responses over Europe–West Asia and Northeast Asia are approximately 0.65°C and 0.47°C, respectively. We then utilize the three AGCMs to estimate the contribution of the AMO-triggered SRP to the AMO-related nonuniform warming. The result indicates a rate of 30% or so by the AMO (35.86%, 31.87% and 35.23% in AM2, CCM3 and GFS, respectively).

It is worthwhile pointing out that this study did not consider the effects of the negative phase AMO. Whether symmetric, inverted nonuniform SAT anomalies will be obtained for the cold period of the AMO is unclear. Wang et al. (2010)

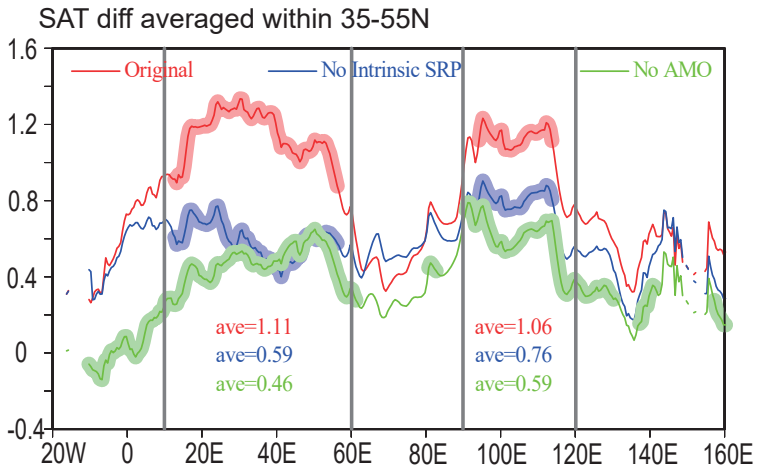

Fig. 13. The JJA-mean SAT differences (1997–2015 minus 1979–96) averaged within 35°–55°N. The red line is for the original temperature, the blue line is for the temperature without the intrinsic SRP-related component, and the green line is for the temperature without the AMO-related component. When the values of the blue line or the green line at a particular longitude are 0.3°C cooler than values of the red line at the same longitude, the lines are shaded. The gray lines indicate the marginal longitude of Europe–West Asia (10°–60°E) and Northeast Asia (90°–120°E). The numbers following the "ave=" are the average values of the meridional-mean temperature in Europe–West Asia and Northeast Asia. The colors of the fonts correspond to the lines with the same color.

and Hao et al. (2016) revealed asymmetry in the SAT response with respect to the sign of the AMO, and particularly the impact of positive AMO as being stronger than its counterpart. This implies that the spatial pattern of SAT anomalies induced by the negative AMO may not be the exact opposite to that by the reversed AMO. Nonetheless, this issue deserves further study.

Finally, the preliminary points about how the AMO affects the Eurasian nonuniform warming can be summarized as in Fig. 14. First, the positive-phase AMO causes the Atlantic ITCZ to move northwards with more precipitation in the north to the equator but less in the south. The related diabatic heating excites the Silk Road wave-train over Eurasia with positive geopotential height and anticyclonic circulation anomalies over Europe and East Asia, but negative geopotential height and cyclonic circulation over Central Asia. The positive geopotential height anomalies and anticyclonic circulation at the upper troposphere favor more shortwave radiation reaching the ground. In comparison, the atmospheric circulation anomaly over Central Asia favors the occurrence of more precipitation and obstructs the shortwave radiation flux. Besides, the vertically averaged temperature advection causes warming in Europe–West Asia and East Asia but cold conditions in Central Asia. When these effects overlap the signals of global warming, it causes amplified warming over Europe to West Asia and over Northeast Asia, but weak warming over Central Asia.

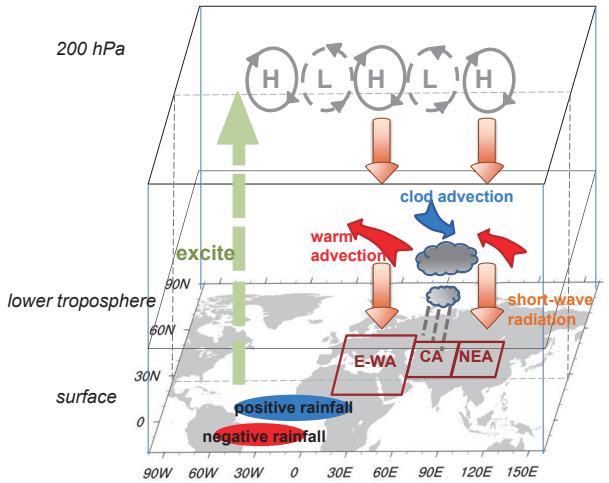

Fig. 14. Schematic diagram illustrating the mechanism of the AMO affecting the Eurasian surface temperature. E-WA, CA and NEA are short for Europe–West Asia, Central Asia and Northeast Asia, respectively.

Acknowledgements. This work was supported by the National Key Research and Development Program of Ministry of Science and Technology of China (Grant 2018YFA0606403 and 2015CB453202).

REFERENCES

Chen, M., P. Xie, J. E. Janowiak, and P. A. Arkin, 2004: Verifying the reanalysis and climate models outputs using a 56-year data set of reconstructed global precipitation. *Proc. 14th AMS Conference on Applied Meteorology*, Washington, Amer. Meteor. Soc.

Enfield, D. B., A. M. Mestas-Nuñez, and P. J. Trimble, 2001: The Atlantic multidecadal oscillation and its relation to rainfall

and river flows in the continental U.S. *Geophys. Res. Lett.*, **28**, 2077–2080, https://doi.org/10.1029/2000GL012745.

Enomoto, T., B. J. Hoskins, and Y. Matsuda, 2003: The formation mechanism of the Bonin high in August. *Quart. J. Roy. Meteor. Soc.*, **129**, 157–178, https://doi.org/10.1256/qj.01.211.

Hagos, S., and Coauthors, 2010: Estimates of tropical diabatic heating profiles: Commonalities and uncertainties. *J. Climate*, **23**, 542–558, https://doi.org/10.1175/2009JCLI3025.1.

Han, Z., F. F. Luo, S. L. Li, Y. Q. Gao, T. Furevik, and L. Svendsen, 2016: Simulation by CMIP5 models of the Atlantic multidecadal oscillation and its climate impacts. *Adv. Atmos. Sci.*, **33**(12), 1329–1342, https://doi.org/10.1007/s00376-016-5270-4.

Hao, X., S. P. He, and H. J. Wang, 2016: Asymmetry in the response of central Eurasian winter temperature to AMO. *Climate Dyn.*, **47**(7–8), 2139–2154, https://doi.org/10.1007/s00382-015-2955-9.

Harris, I., P. D. Jones, T. J. Osborn, and D. H. Lister, 2014: Updated high-resolution grids of monthly climatic observations—The CRU TS3.10 dataset. *International Journal of Climatology*, **34**, 623–642, https://doi.org/10.1002/joc.3711.

Hong, X. W., and R. Y. Lu, 2016: The meridional displacement of the summer Asian jet, silk road pattern, and tropical SST anomalies. *J. Climate*, **29**, 3753–3766, https://doi.org/10.1175/JCLI-D-15-0541.1.

Hong, X. W., R. Y. Lu, and S. L. Li, 2017: Amplified summer warming in Europe-West Asia and Northeast Asia after the mid-1990s. *Environmental Research Letters*, **12**, 094007, https://doi.org/10.1088/1748-9326/aa7909.

Ionita, M., G. Lohmann, N. Rimbu, S. Chelcea, and M. Dima, 2012: Interannual to decadal summer drought variability over Europe and its relationship to global sea surface temperature. *Climate Dyn.*, **38**(1–2), 363–377, https://doi.org/10.1007/s00382-011-1028-y.

Ionita, M., N. Rimbu, S. Chelcea, and S. Patrut, 2013: Multidecadal variability of summer temperature over Romania and its relation with Atlantic multidecadal oscillation. *Theor. Appl. Climatol.*, **113**(1–2), 305–315, https://doi.org/10.1007/s00704-012-0786-8.

Jin, F. F., and B. J. Hoskins, 1995: The direct response to tropical heating in a baroclinic atmosphere. *J. Atmos. Sci.*, **52**, 307–319, https://doi.org/10.1175/1520-0469(1995)052<0307:TDRTTH>2.0.CO;2.

Kalnay, E., and Coauthors, 1996: The NCEP/NCAR 40-year reanalysis project. *Bull. Amer. Meteor. Soc.*, **77**(3), 437–472, https://doi.org/10.1175/1520-0477(1996)077<0437:TNYRP>2.0.CO;2.

Kaplan, A., M. A. Cane, Y. Kushnir, A. C. Clement, M. B. Blumenthal, and B. Rajagopalan, 1998: Analyses of global sea surface temperature 1856–1991. *J. Geophys. Res.*, **103**, 18 567–18 589, https://doi.org/10.1029/97JC01736.

Knight, J. R., C. K. Folland, and A. A. Scaife, 2006: Climate impacts of the Atlantic multidecadal oscillation. *Geophys. Res. Lett.*, **33**, L17706, https://doi.org/10.1029/2006GL026242.

Kosaka, Y., J. S. Chowdary, S. P. Xie, Y. M. Min, and J. Y. Lee, 2012: Limitations of seasonal predictability for summer climate over East Asia and the northwestern Pacific. *J. Climate*, **25**, 7574–7589, https://doi.org/10.1175/JCLI-D-12-00009.1.

Li, S. L., 2004: Impact of Northwest Atlantic SST Anomalies on the Circulation over the Ural Mountains during Early Winter. *J. Meteor. Soc. Japan*, **82**, 971–988.

Li, S. L., and G. T. Bates, 2007: Influence of the Atlantic multidecadal oscillation on the winter climate of East China. *Adv. Atmos. Sci.*, **24**(1), 126–135, https://doi.org/10.1007/s00376-007-0126-6.

Li, S. L., J. Perlwitz, M. P. Hoerling, and X. T. Chen, 2010: Opposite annular responses of the northern and southern hemispheres to Indian Ocean warming. *J. Climate*, **23**, 3720–3738, https://doi.org/10.1175/2010JCLI3410.1.

Lu, R. Y., J. H. Oh, and B. J. Kim, 2002: A teleconnection pattern in upper-level meridional wind over the North African and Eurasian continent in summer. *Tellus*, **54**, 44–55, https://doi.org/10.1034/j.1600-0870.2002.00248.x.

Mohino, E., S. Janicot, and J. Bader, 2011: Sahel rainfall and decadal to multi-decadal sea surface temperature variability. *Climate Dyn.*, **37**(3–4), 419–440, https://doi.org/10.1007/s00382-010-0867-2.

Peng, S. L., and J. S. Whitaker, 1999: Mechanisms determining the atmospheric response to midlatitude SST anomalies. *J. Climate*, **12**, 1393–1408, https://doi.org/10.1175/1520-0442(1999)012<1393:MDTART>2.0.CO;2.

Shao, X. L., S. L. Li, N. Liu, and J. Song, 2018: The Madden–Julian oscillation during the 2016 summer and its possible impact on rainfall in China. *International Journal of Climatology*, **38**, 2575–2589, https://doi.org/10.1002/joc.5440.

Sun, J. Q., H. J. Wang, and W. Yuan, 2008: Decadal variations of the relationship between the summer North Atlantic Oscillation and middle East Asian air temperature. *J. Geophys. Res.*, **113**, D15107, https://doi.org/10.1029/2007JD009626.

Ting, M. F., and S. L. Peng, 1995: Dynamics of the early and middle winter atmospheric responses to the northwest Atlantic SST anomalies. *J. Climate*, **8**, 2239–2254, https://doi.org/10.1175/1520-0442(1995)008<2239:DOTEAM>2.0.CO;2.

Ting, M. F., Y. Kushnir, R. Seager, and C. H. Li, 2009: Forced and internal Twentieth-century SST trends in the North Atlantic. *J. Climate*, **22**, 1469–1481, https://doi.org/10.1175/2008JCLI2561.1.

Ting, M. F., Y. Kushnir, R. Seager, and C. H. Li, 2011: Robust features of Atlantic multi-decadal variability and its climate impacts. *Geophys. Res. Lett.*, **38**, L17705, https://doi.org/10.1029/2011GL048712.

Wang, Y. M., S. L. Li, and D. H. Luo, 2009: Seasonal response of Asian monsoonal climate to the Atlantic multidecadal oscillation. *J. Geophys. Res.*, **114**, D02112, https://doi.org/10.1029/2008JD010929.

Wang, Y. M., S. L. Li, D. H. Luo, and J. J. Fu, 2010: Nonlinearity in the Asian monsoonal climate response to Atlantic multidecadal oscillation. *Periodical of Ocean University of China*, **40**(6), 19–26, https://doi.org/10.16441/j.cnki.hdxb.2010.06.003. (in Chinese)

Yanai, M., S. Esbensen, and J. H. Chu, 1973: Determination of bulk properties of tropical cloud clusters from large-scale heat and moisture budgets. *J. Atmos. Sci.*, **30**, 611–627, https://doi.org/10.1175/1520-0469(1973)030<0611:DOBPOT>2.0.CO;2.

Zhang, R., and T. L. Delworth, 2006: Impact of Atlantic multidecadal oscillations on India/Sahel rainfall and Atlantic hurricanes. *Geophys Res Lett.*, **33**(17), L17712, https://doi.org/10.1029/2006GL026267.